ACS OMEGA

Open Access

http://pubs.acs.org/journal/acsodf

Article

Resveratrol-Coated Gold Nanoflowers for CT Imaging and Apoptosis/Photothermal Synergistic Therapy of Malignant Melanoma

Tianye Yang, Hui Ren, Wei Zhang, Li Rong,* and Duo Zhang*

Cite This: *ACS Omega* 2023, 8, 34629−34639

Read Online

ACCESS | Metrics & More | Article Recommendations | Supporting Information

ABSTRACT: In the past decade, photothermal therapy (PTT) of tumors based on gold nanomaterials has been widely studied because of their strong extinction ability and high photothermal conversion ability in the near-infrared (NIR) region. However, related research still faces two problems: First, the biosafety of the surface ligands on gold nanomaterials is not ideal and even has strong toxicity, so the surface modification or shell coating is very necessary; second, gold nanomaterials only have a single PTT function, which requires high temperature to achieve better treatment effect. Therefore, it is necessary to enrich the antitumor function of gold nanomaterials and realize synergistic therapy. Natural polyphenols can combine with each other or other substances through various supramolecular forces, forming shells on the surface of nanomaterials and reducing biotoxicity. In addition, natural polyphenols represented by resveratrol have antitumor activity and can induce apoptosis of tumor cells. Therefore, the surface coating method of gold nanomaterials with natural polyphenols with antitumor activity can effectively solve the above problems. In this work, we prepared resveratrol-coated gold nanoflowers (Au@Res NFs) and applied them to the treatment of malignant melanoma. Resveratrol in Au@Res NFs can induce the apoptosis of tumor cells, and Au@Res NFs can play a role in PTT under an NIR laser. In cell experiments, the synergistic effect of apoptosis/PTT on the A375 cells was extremely strong. In animal experiments, Au@Res NFs enriched in tumor sites identified the location and boundary of tumors by computed tomography (CT). The apoptosis induced by resveratrol had a certain inhibitory effect on tumor growth. Further applying the NIR laser, under the synergistic effect of apoptosis and PTT, the tumors were completely eliminated without recurrence during the experimental period.

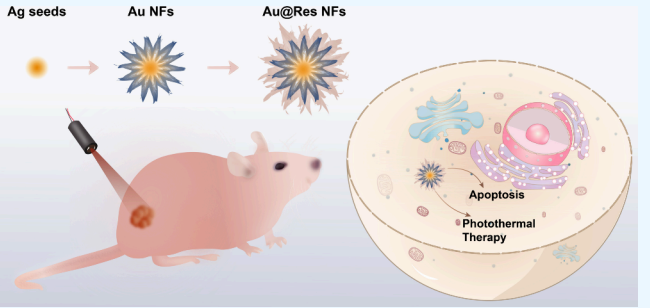

INTRODUCTION

In the past decade, nanoscience and nanotechnology have developed rapidly and brought about many positive effects on human life.[1−3] In the field of biomedicine, nanomaterial-based photothermal therapy (PTT),[4,5] photodynamic therapy (PDT),[6,7] sonodynamic therapy (SDT),[8,9] chemodynamic therapy (CDT),[10−13] immunotherapy,[14,15] and other new methods[16,17] have greatly promoted the development of tumor treatment methodology and provided more possibilities for tumor therapy.[18]

Among many nanomaterials, gold nanomaterials are chemically inert and have good stability and high biocompatibility *in vivo*.[19,20] Gold nanomaterials have a high X-ray absorption coefficient and can be used as contrast agents in computed tomography (CT).[21] Besides, due to the local surface plasmon resonance effect, the absorption spectrum of gold nanomaterials is red-shifted. Therefore, the extinction ability of gold nanomaterials in the near-infrared (NIR) region is enhanced and the photothermal conversion ability is good.[22]

Gold nanomaterials such as gold nanospheres,[23,24] gold nanorods,[25,26] gold nanocages,[27,28] and gold nanoflowers (Au NFs),[29,30] are widely used in the PTT of tumors. However, the application of gold nanomaterials in tumor treatment is also limited by some factors, mainly reflected in two aspects: on the one hand, the preparation process of gold nanomaterials mostly uses surface ligands, which are not ideal in biological safety and even have strong toxicity;[31] on the other hand, the treatment function of gold nanomaterials is single, simple PTT requires higher temperature to achieve better treatment effect, and high temperature is easy to burn skin and tissues, bringing additional damage to organisms.[32] Therefore, coating gold nanomaterials with antitumor substances can not only reduce the potential toxicity of the ligands on the surface of gold nanomaterials but also contribute to the realization of tumor synergistic therapy.[33]

Received: May 21, 2023
Accepted: September 5, 2023
Published: September 14, 2023

https://doi.org/10.1021/acsomega.3c03538
ACS Omega 2023, 8, 34629−34639

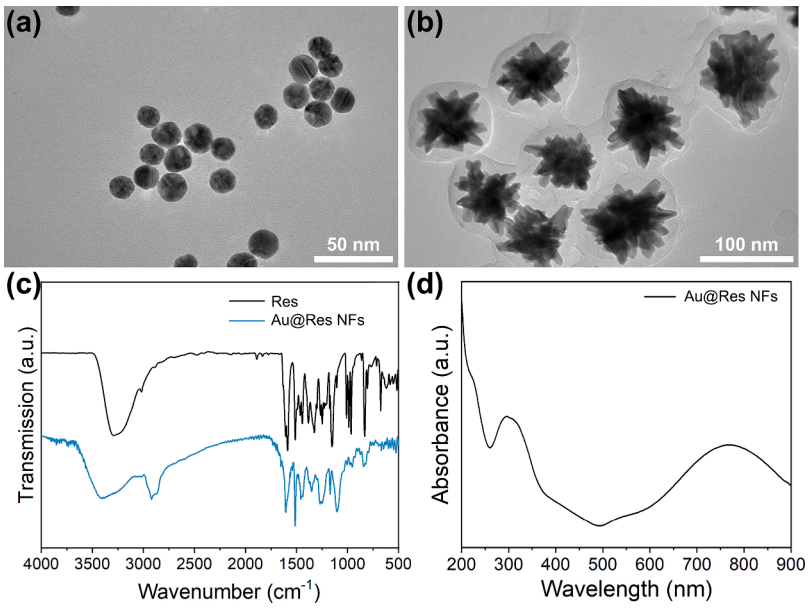

Figure 1. (a) TEM image of Au seeds. (b) TEM image of Au@Res NFs. (c) FTIR spectra of Res and Au@Res NFs. (d) UV−vis-NIR absorption spectra of Au@Res NFs.

Natural polyphenols are a kind of compounds widely existing in animals and plants, which have antitumor, antioxidation, antibacterial, and other biological effects and are widely used in the treatment of various diseases.[34−36] For example, resveratrol can lead to the reduction of mitochondrial membrane potential, induce mitochondrial damage and cell cycle arrest, and play an antitumor effect through apoptosis.[37] In addition, natural polyphenols can be combined with each other or other substances through various supramolecular forces, such as coordination, $\pi-\pi$ interaction, hydrophobic interaction, and hydrogen bonding; moreover, they can not only form nanoparticles, films, hydrogels, and other materials but also be used as surface shells to coat inorganic nanomaterials.[38] This can not only retain the activity of natural polyphenols but also improve their water solubility, which is helpful to playing a better biological role.

In this work, we used resveratrol as a reducing agent to prepare core−shell composite nanoparticles with Au NFs as the core and resveratrol as the shell (Au@Res NFs). Au@Res NFs have strong absorption in the NIR region, and the photothermal conversion efficiency is up to 36.9%. The coating of the resveratrol shell greatly reduces the toxicity of ligands on the surface of Au NFs, and the biosafety of Au@Res NFs is good. In cell experiments, Au@Res NFs induced the apoptosis of the A375 cells. The cell cycle was arrested in the S phase, the proliferation ability were weakened, the expression of antiapoptotic proteins was downregulated, and the expression of pro-apoptotic proteins was up-regulated. In addition, Au@Res NFs also absorbed NIR light to generate heat, which further achieved the effect of PTT. Under 808 nm laser irradiation, the survival rate of A375 cells was significantly reduced and the synergistic effect of apoptosis and PTT on A375 cells was significant. In animal experiments, Au@Res NFs accumulated in tumors on account of EPR effect and the retention rate is up to 6.2%ID/g. Because of the high X-ray absorption coefficient of gold, Au@Res NFs enriched in the tumors can be used as a contrast agent in CT imaging to localize malignant melanoma. Resveratrol in Au@Res NFs can induce the apoptosis of A375 cells and inhibit tumor growth. Further applying NIR laser, under the synergistic effect of apoptosis and PTT, the A375 tumor was completely eliminated without recurrence in the experimental period. Hematological and histological studies confirmed the safety of the experiment.

RESULTS AND DISCUSSION

In this work, the classical seed growth method was used for the synthesis of nanomaterials. As shown in transmission electron microscopy (TEM) photos, Au seeds with uniform morphology were first prepared and their average diameter was 11.6 nm (Figure 1a). Using Au seeds as templates, Au NFs were then prepared. Au NFs also showed a uniform size distribution, with an average diameter of 81.2 nm. By further coating the resveratrol shell on the surface of Au NFs, Au@Res NFs were successfully prepared and the average shell thickness was 7.5 nm (Figure 1b). The characteristic peaks belonging to resveratrol also appeared in the Fourier transform infrared (FTIR) spectra of Au@Res NFs, which proved the successful coating of the resveratrol shell (Figure 1c). The mass fraction of resveratrol in Au@Res NFs is 9.0%. XRD patterns show that the crystal structure of Au NFs was not affected by the coating of resveratrol (Figure S1). The coating of the resveratrol shell also gave nanomaterial a positive surface charge, and the zeta potential of Au@Res NFs was measured as +17.4 ± 2.6 mV. In addition, due to the local surface plasmon resonance (LSPR) effect of gold nanomaterials, Au@Res NFs exhibited high extinction ability at 808 nm and can be applied to PTT (Figure 1d).

To study photothermal performance, the temperature increments of Au@Res NF aqueous solutions under 808 nm laser were measured. At a fixed concentration of 100 μg/mL, the solution temperature increased with laser power density on account of increased dose of irradiation (Figure 2a). Similarly, when the concentration was fixed at 200 μg/mL, the solution temperature also increased with laser power density (Figure 2b). Then, under the experimental conditions of a concentration of 200 μg/mL and laser power density of 3 W/cm^2, the rising and cooling data of solution were used to calculate the

https://doi.org/10.1021/acsomega.3c03538
ACS Omega 2023, 8, 34629−34639

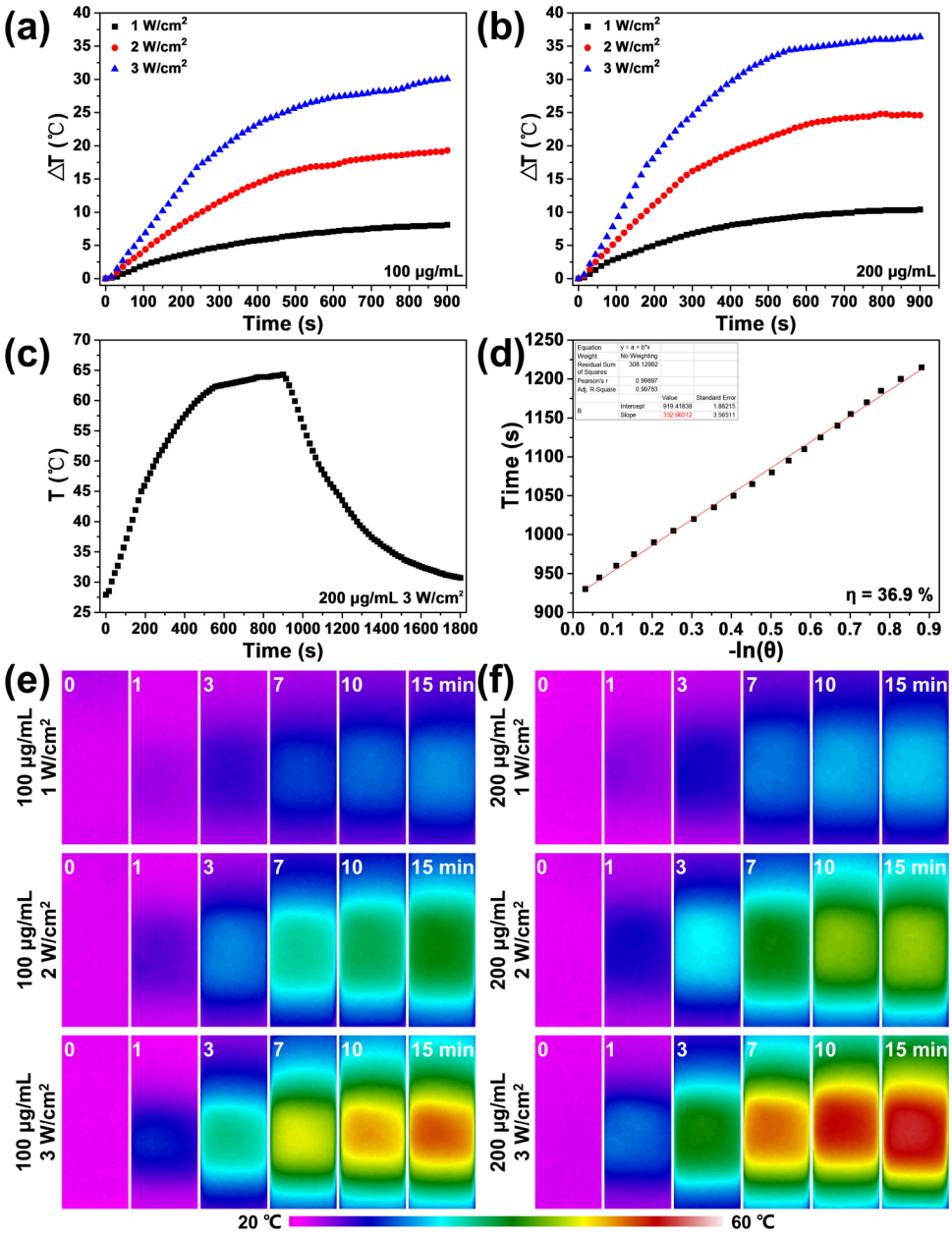

Figure 2. (a) Temperature increments of Au@Res NF solutions at 100 μg/mL irradiated by an 808 nm laser at different power densities of 1, 2, and 3 W/cm^2. (b) Temperature increments of Au@Res NF solutions at 200 μg/mL irradiated by 808 nm laser at different power densities of 1, 2, and 3 W/cm^2. (c) The heating−cooling process of Au@Res NF solution at 200 μg/mL irradiated by an 808 nm laser at the power density of 3 W/cm^2, and the laser was removed at 900 s when the solution reached maximum temperature. (d) The linear time versus the negative natural logarithm of driving force temperature during the cooling period. The time constant for heat transfer: τ_s = 332.96 s. The photothermal conversion efficiency: η = 36.9%. (e) Infrared thermal images of Au@Res NF solutions at 100 μg/mL irradiated by an 808 nm laser at different power densities of 1, 2, and 3 W/cm^2. (f) Infrared thermal images of Au@Res NF solutions at 200 μg/mL irradiated by an 808 nm laser at different power densities of 1, 2, and 3 W/cm^2.

photothermal conversion efficiency of Au@Res NFs. Through calculation, the photothermal conversion efficiency was 36.9% (Figure 2c,d), which is not only higher than the average level of gold nanomaterials[33] but also basically at the same level compared with the reported photothermal reagents based on Au NFs[38,39] and has strong competitiveness. A thermal infrared imager was also employed to monitor the solution temperature. Similar to the data given in Figure 2a,b, the infrared thermal imaging images also show that the temperature of the Au@Res NF solution increased with the increase of the laser power density (Figure 2e,f). It is worth noting that a higher laser power density was selected in the above experiment, in order to avoid the influence of heat loss of solution on the accuracy of the experiment caused by too long of an experiment time.

Before biomedical applications, the colloidal stability of nanomaterials was studied first. Au@Res NFs were well dispersed and stable in water, saline, PBS, and cell culture medium. Even after 7 days of incubation, there was only a slight settlement under gravity, which could be redispersed by slight shaking (Figure S2). The Au@Res NFs after 24 h of incubation in cell culture medium still maintained their original

https://doi.org/10.1021/acsomega.3c03538
ACS Omega 2023, 8, 34629−34639

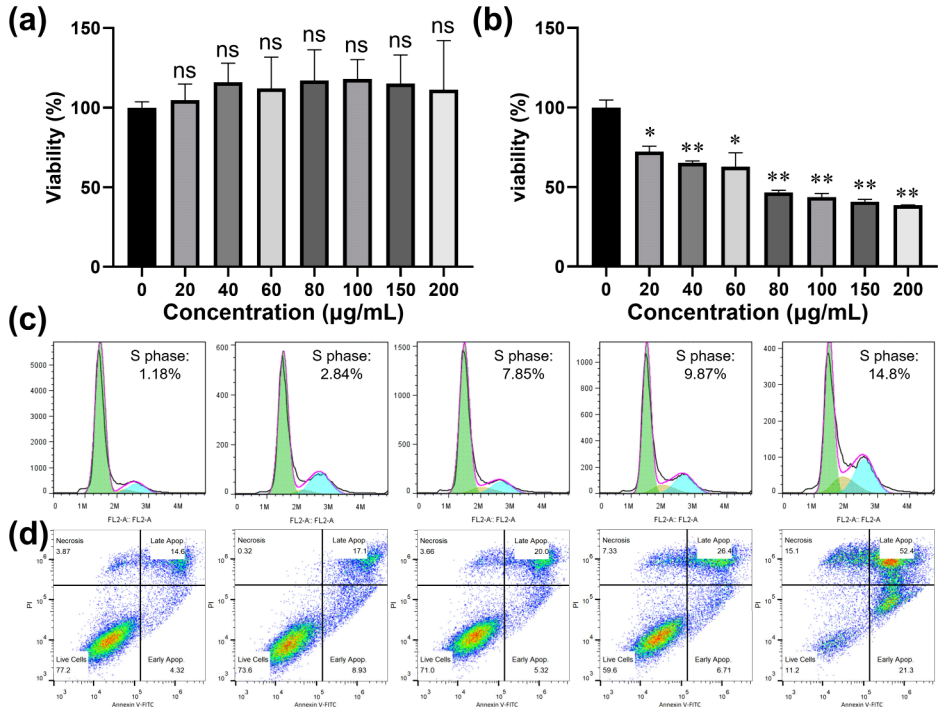

Figure 3. L929 cells (a) and A375 cells (b) were incubated with Au@Res NFs at different concentrations of 0, 20, 40, 60, 80, 100, 150, and 200 μg/mL for 24 h, and the cell viabilities were obtained by the CCK-8 assay. Each experiment was repeated five times. Data are shown as mean ± standard deviation (SD), with ns (no significance), * ($p < 0.05$), and ** ($p < 0.01$). (c) A375 cells were incubated with Au@Res NFs at different concentrations of 0, 25, 50, 75, and 100 μg/mL for 24 h. The cell cycle was obtained by flow cytometry, and 10^4 of cells were counted. Each experiment was repeated three times. (d) A375 cells were incubated with Au@Res NFs at the concentration of 50 μg/mL, and then the cells were irradiated with 808 nm laser at different power densities of 0, 0.33, 0.5, 1, and 2 W/cm^2. After 24 h incubation, the cell apoptosis was obtained by flow cytometry and 10^4 of cells were counted. Each experiment was repeated three times.

hydrated particle size and did not aggregate (Figure S3). Therefore, the colloidal stability of Au@Res NFs was very good.

Then, the cytotoxicity *in vitro* was evaluated by the cell counting kit-8 (CCK-8) assay. The killing effect of Au@Res NFs on L929 cells is much lower than that of Au NFs (Figure 3a, Figure S4). Au@Res NFs have no obvious cytotoxicity at concentrations up to 200 μg/mL, because the coating of the resveratrol shell improves the biosafety of nanomaterials. However, the viability of A375 cells decreased gradually with an increased concentration. At the Au@Res NF concentration of 200 μg/mL, the cell viability was lower than 40% (Figure 3b). The killing effect of Au@Res NFs came from the resveratrol shell. As the concentration of resveratrol cocultured with A375 cells increased, the cell viability gradually decreased because resveratrol arrested the cell cycle in the S phase and induced apoptosis (Figure S5). As shown in Figure 3c and Table S1, with the increase of the Au@Res NF concentration, the proportion of A375 cells in the S phase gradually increased because the increased Au@Res NFs in A375 cells also increased the content of intracellular resveratrol. The apoptosis caused by Au@Res NFs was also reflected in the change of protein expression level in cells. After incubating with Au@Res NFs at different concentrations, the expressions of Bax protein associated with promoting cell apoptosis and Bcl2 protein associated with inhibiting cell apoptosis were significantly changed. With the increase of the Au@Re NF concentration, the expression of Bax protein was up-regulated in A375 cells while the expression of Bcl2 protein was downregulated (Figure S6). All the studies indicated that the Au@Res NFs can induce the apoptosis of the A375 cell.

It is also important to note that apoptosis alone is not sufficient to efficiently kill tumor cells. Therefore, an NIR laser with 808 nm wavelength was further applied to exert the effect of PTT. After being incubated with Au@Res NFs at the concentration of 50 μg/mL, A375 cells were irradiated by 808 nm at different power densities of 0, 0.33, 0.5, 1, and 2 W/cm^2. Then, the killing effect of Au@Res NFs on A375 was evaluated by flow cytometry (dyes: Annexin V-FITC and PI). As shown in Figure 3d, the percentage of live cells decreased gradually attributed to the increased efficacy of PTT. When the laser power density reached 2 W/cm^2, the proportion of living cells is only 11.2%. To be clear, even if a few cells were kept alive, their proliferation ability was greatly impaired. Clone formation assay showed that the higher the power density of A375 cells subjected to laser irradiation, the lower the proliferation ability, which was reflected in the gradual reduction of the number of cell colonies (Figure S7). In summary, apoptosis/photothermal synergistic therapy is effective for killing A375 cells. Even a small number of A375 cells could still survive after synergistic therapy, but their proliferation ability was basically lost.

Before the synergistic therapy experiments *in vivo*, the biosafety of Au@Res NFs was first investigated. Mice intravenously injected with 50 μL of Au@Res NF solution were used as the experimental group, and healthy mice intravenously injected with 50 μL of saline were used as the control group. After 24 h, the blood of all the mice was collected for blood glucose, blood fat, liver function, and renal function examinations. There was no obvious difference in the blood glucose index between the experimental group and the control group (Figure S8). Similarly, blood fat indexes such as

https://doi.org/10.1021/acsomega.3c03538
ACS Omega 2023, 8, 34629−34639

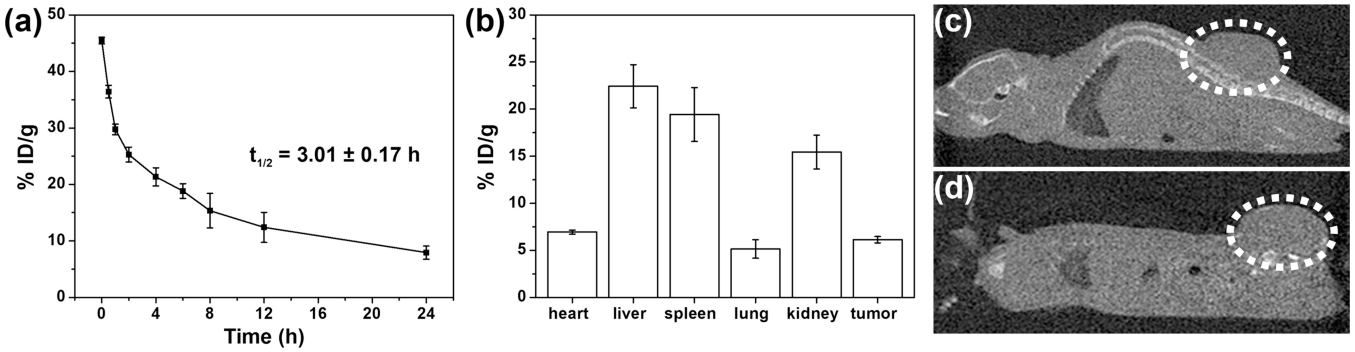

Figure 4. (a) Blood circulation of Au@Res NFs *in vivo*. (b) Biodistribution of Au@Res NFs in major organs and tumor 24 h after the injection. % ID means the amount of Au@Res NFs in the sample as a percentage of the total amount injected. Sagittal CT images of A375 tumor-bearing Balb/c nude mice 24 h after the injection of saline (c) and Au@Res NF solution (d).

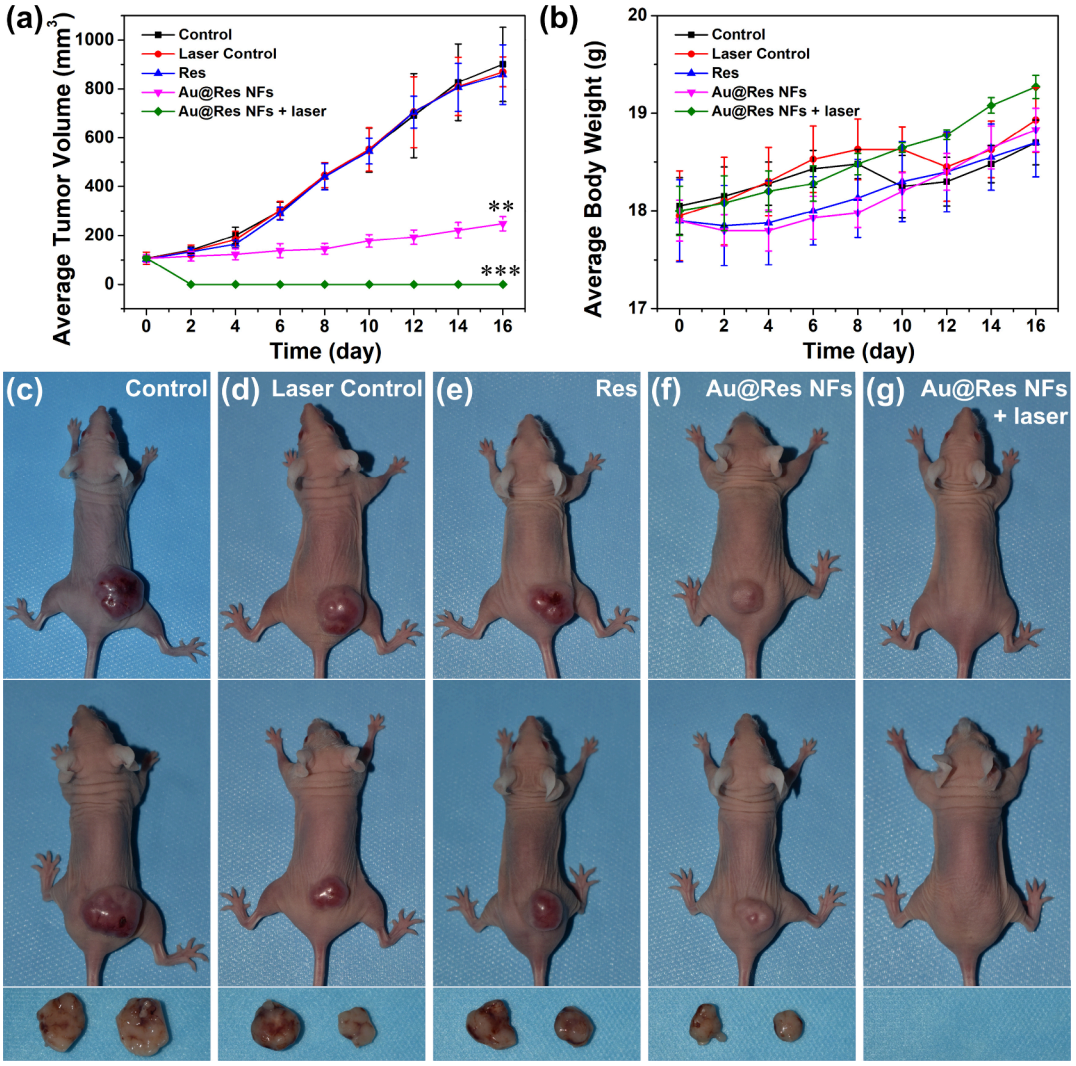

Figure 5. Apoptosis/photothermal synergistic therapy *in vivo*. The A375 tumor-bearing Balb/c nude mice are divided into five groups: control group, Laser control group, Res group, Au@Res NF group, and Au@Res NFs + laser group. (a) Average tumor volume curves for each group. Data are shown as mean ± standard deviation (SD), with ** ($p < 0.01$) and *** ($p < 0.001$). (b) Average body weight curves for each group. (c–g) Photographs of typical mice and tumors at the end of treatment for each group. The average tumor volumes are 900.7 ± 151.5, 869.6 ± 60.9, 858.5 ± 122.1, 248.0 ± 28.7, and 0 mm^3, respectively. The two tumors were the largest and smallest ones in the groups.

total cholesterol (CHOL), triglyceride (TG), high-density lipoprotein (HDL), and low-density lipoprotein (LDL) were all at very similar levels (Figure S9). Besides, the main liver function indexes such as aspartate transaminase (AST), alanine aminotransferase (ALT), alkaline phosphatase (ALP), cholinesterase (CHE), and albumin (ALB) in the experimental group, and the main renal function indexes such as blood urea nitrogen (BUN), creatinine (CREA), and uric acid (UA) in

https://doi.org/10.1021/acsomega.3c03538
ACS Omega 2023, 8, 34629−34639

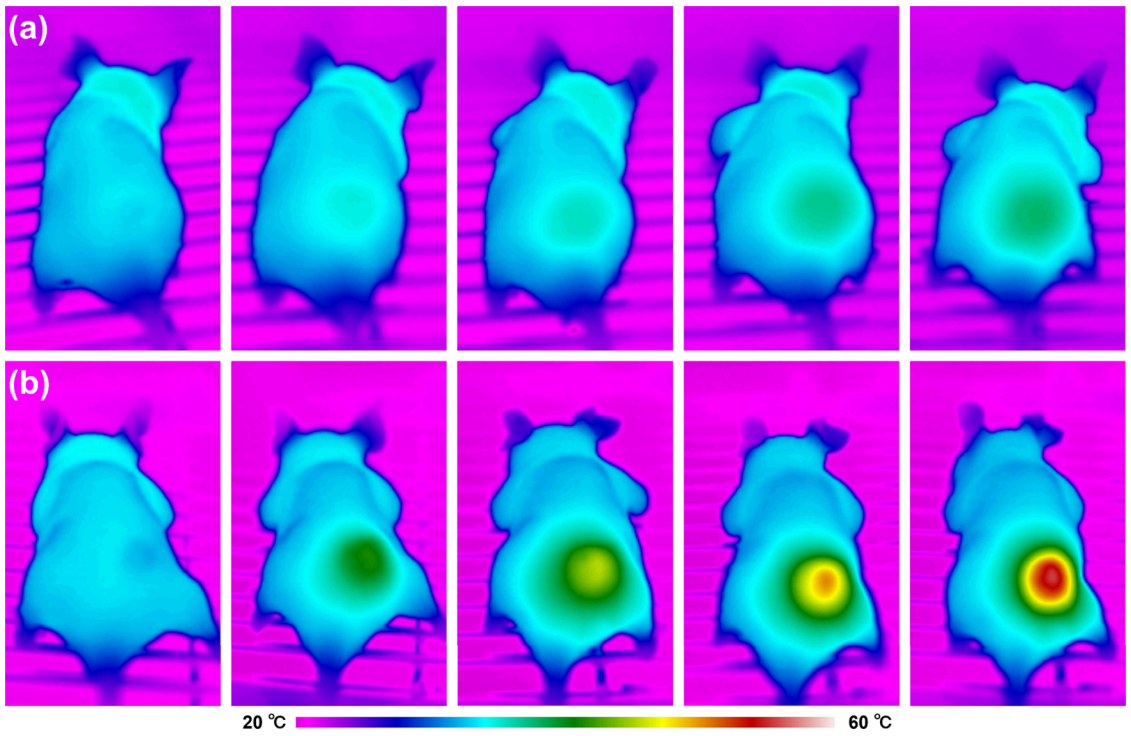

Figure 6. IR thermal images of A375 tumor-bearing Balb/c nude mice treated with saline + laser (a) and Au@Res NFs + laser (b). The laser power density is 0.33 W/cm^2, and the irradiation times are 0, 5, 10, 20, and 30 min, respectively.

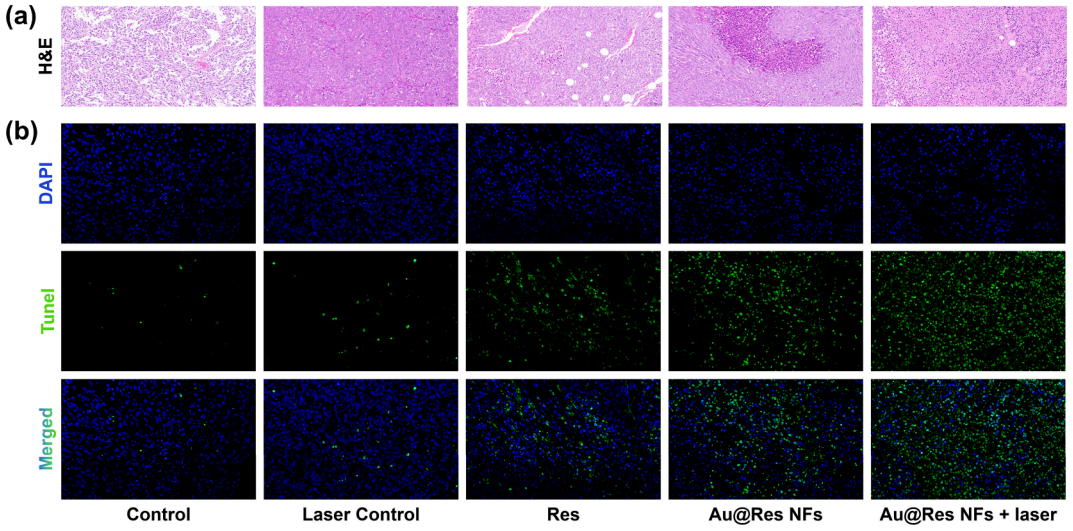

Figure 7. H&E-stained (a) and TUNEL-stained (b) tumor slices of each group (magnification: 200×).

the experimental group were at the same level as those in the control group (Figure S10, S11). The above four experiments show that Au@Res NFs had good biosafety *in vivo*.

Then, the pharmacokinetic behavior of Au@Res NFs was systematically studied. By monitoring the amount of Au in the blood with an inductively coupled plasma-atomic emission spectrometer (ICP-AES), the concentration of Au@Res NFs in the blood over time can be measured. The content of Au@Res NFs in blood showed a tendency to decay with time, and the blood circulation half-life ($t_{1/2}$) was 3.01 ± 0.17 h (Figure 4a). The relatively long half-life was conducive to the accumulation of nanoparticles into the tumor site. 24 h after the intravenous injection, the accumulation rate of Au@Res NFs in the A375 tumor was 6.13 ± 0.34%ID/g, which is relatively high (Figure 4b). At the same time, Au@Res NFs were also accumulated in the liver (22.43 ± 2.29%ID/g) and spleen (19.43 ± 2.86%ID/g), which is the result of the reticuloendothelial system (RES).

The Au in Au@Res NFs had a high X-ray absorption coefficient and can be used as a contrast agent for CT imaging. Therefore, the accumulation behavior of Au@Res NFs in A375 tumors can be used for tumor localization. As shown in Figure 4c, in A375 tumor-bearing mice injected with saline through the tail vein, the CT signal intensity of the tumor site was basically maintained close to that of muscle tissue. After the injection of Au@Res NFs, the CT signal intensity at the tumor site of mice was significantly enhanced, and not only did the

https://doi.org/10.1021/acsomega.3c03538
ACS Omega 2023, 8, 34629−34639

average intensity increase but also multiple high signal points appeared, showing white enhancement (Figure 4d).

The increased content of Au@Res NFs in the tumor site was helpful for the play of therapeutic function. As shown in Figure 5a, the Au@Res NFs significantly reduced the growth rate of A375 tumors. In contrast, the tumors in the control group and the laser control group maintained rapid growth, reaching an average volume of up to 900.7 ± 151.5 and 869.6 ± 60.9 mm^3 after a 16-day experimental period (Figure 5a,c,d). Besides, resveratrol molecules can be excreted to the outside of the body quickly through the kidney, which was not conducive to the play of the drug effect, and the influence on tumor growth was very low. The average tumor volume was 858.5 ± 122.1 mm^3 after the same 16-day experimental period (Figure 5a,e). Au@Res NFs inhibited tumor growth not only in the growth curve but also in the reduction of the average tumor volume. The average tumor volume was only 248.0 ± 28.7 mm^3, and the tumor inhibition rate reached 72.5% (Figure 5f). It is also important to note that Au@Res NFs, while effective in inhibiting tumor growth, did not eliminate the tumor completely. Therefore, the NIR laser was further applied to exert the efficacy of PTT. NIR lasers can cause a rapid temperature rise at the tumor site. After 30 min of 0.33 W/cm^2 laser irradiation, the temperature at the tumor site exceeded 50 °C, which was enough to cause the death of tumor cells in a large area (Figure 6b). After treatment, the tumors were completely eliminated without recurrence (Figure 5g). In contrast, the increase in temperature was very low in the laser control group without the Au@Res NFs, suggesting that the laser alone was not enough to kill cancer cells, consistent with the experimental results shown in the laser control group (Figures 5a,d and 6a).

Histological methods were used to further evaluate the effect of treatment (Figure 7a,b). Hematoxylin and eosin (H&E)-stained tumor sections showed almost no significant cell death in the control group and the laser control group, and TUNEL staining showed a very low percentage of apoptotic cells. The degree of apoptosis of tumor cells in the Res group was also at a low level, which also indicated that the therapeutic effect of resveratrol molecules was limited. The accumulation of Au@Res NFs into A375 tumors under the EPR effect was conducive to the increase of resveratrol content in tumors. Therefore, tumor cells in the group of Au@Res NFs had a large area of apoptosis. After further application of near-infrared laser, the degree of apoptosis of tumor cells was further improved and the synergistic effect of apoptosis and PTT was obviously superior to the single effect of apoptosis.

The weight of the mice also varied from group to group. In the control group, laser control group, Res group, and Au@Res NF group, the weight of mice fluctuated, which proved that the growth of tumor had a certain impact on the health of mice, especially in the control group the fluctuation was the most obvious. In the group Au@Res NFs + laser, the synergistic effect of apoptosis and PTT led to complete tumor elimination. Without the effect of tumor growth on the metabolism of mice, the body weight of mice showed a steady increase, which reflected the safety of our experiment (Figure 5b). In addition, H&E staining photos of major organs (including heart, liver, spleen, lung, and kidney) of nude mice before and after the experiment showed that all tissues were in normal morphology and structure, without inflammation, necrosis, etc., which also proved the good safety of our experiment (Figure S12).

CONCLUSIONS

In conclusion, we successfully designed and prepared the Au@Res NFs with the functions of CT imaging, apoptosis, and PTT and successfully achieved the treatment of A375 tumor. The resveratrol coating on Au@Res NFs greatly reduced the toxicity and improved the biosafety. Moreover, the Au in Au@Res NFs had strong absorption in the NIR region and the photothermal conversion efficiency was as high as 36.9%. In cell experiments, Au@Res NFs blocked the cell cycle in the S phase and induced the apoptosis of A375 cells. After applying a further 808 nm laser, the survival rate of A375 cells continued to decrease significantly and the synergistic effect of apoptosis and PTT on A375 cells was significant. In animal experiments, the Au@Res NFs accumulated in tumors not only served as a CT imaging contrast agent to locate the tumor but also achieved the treatment of A375 tumor through the synergistic effect of apoptosis and PTT. Hematological and histological studies confirmed the biosafety of our experiment jointly.

EXPERIMENTAL SECTION

Materials. Tetrachloroauric acid tetrahydrate ($HAuCl_4 \cdot 4H_2O$), sodium citrate, silver nitrate ($AgNO_3$), C_2H_5OH, formaldehyde, and $NH_3 \cdot H_2O$ were purchased from Sinopharm Chemical Reagent Company. Hydroquinone and resveratrol were purchased from Sigma-Aldrich. The CCK-8 kit, cell cycle and apoptosis analysis kit, SDS-PAGE gel quick preparation kit, BCA protein assay kit, QuickBlock blocking buffer for Western blot, and hypersensitive ECL chemiluminescence kit were purchased from Beyotime. Dulbecco's Modified eagle's medium (DMEM) with the D-glucose content of 4.5 g/L and the Annexin V-FITC/PI apoptosis detection kit were purchased from Beijing Solarbio Science & Technology Co., Ltd. Fetal bovine serum (FBS) was purchased from Biological Industries (BI). DMEM containing 10% FBS was used in all experiments. Bax polyclonal antibody, Bcl2 polyclonal antibody, β-tubulin polyclonal antibody, and HRP-labeled goat anti-rabbit IgG H&L were purchased from Proteintech.

Preparation of Au Seeds. $HAuCl_4 \cdot 4H_2O$ was dissolved in water to prepare a solution with a concentration of 100 mM. Sodium citrate was dissolved in water to prepare a solution with a concentration of 10 mg/mL. Then, 520 μL of 100 mM $HAuCl_4 \cdot 4H_2O$ solution was made up to 200 mL with water and the solution was heated in a conical flask. After boiling, 10 mL of sodium citrate solution was added to the above solution and kept boiling for 20 min and then the Au seeds were prepared.

Preparation of Au NFs. 400 μL of Au seed solution, 80 μL of $HAuCl_4 \cdot 4H_2O$ solution (100 mM), 80 μL of $AgNO_3$ solution (1 mg/mL), and 1 mL of hydroquinone solution (30 mM) were added into 10 mL of deionized water at room temperature. After stirring for 30 min, the mixed solution was centrifuged at the speed of 5000 rpm for 10 min. The precipitates were washed with deionized water, and then Au NFs were obtained for further use.

Preparation of Au@Res NFs. 3 mL of C_2H_5OH, 30 μL of formaldehyde, 100 μL of $NH_3 \cdot H_2O$, and 275 μL of resveratrol ethanol solution (20 mg/mL) were added into the as-prepared Au NF solution. After stirring for 1 h, the mixed solution was centrifuged at the speed of 5000 rpm for 10 min. The precipitates were washed with deionized water, and then Au@Res NFs were obtained. A small amount of deionized water was added to prepare a concentrated solution of Au@Res NFs,

https://doi.org/10.1021/acsomega.3c03538
ACS Omega 2023, 8, 34629−34639

and the solution solid content was determined. Finally, according to the needs of subsequent experiments, Au@Res NF solution was diluted to suitable concentrations with deionized water.

Photothermal Performance of Au@Res NFs. A 2 mL amount of Au@Res NF solutions was added to quartz cells. A digital thermometer hanging above the laser path was used to record the temperature of the solutions at an interval of 15 s. At the same time, an infrared thermal camera was also used to photograph the infrared thermal images of the solutions. First, the concentration of Au@Res NF solution was fixed at 100 μg/mL and the solution was irradiated by an 808 nm laser with different power densities of 1, 2, and 3 W/cm^2, respectively. Second, the concentration of Au@Res NF solution was fixed at 200 μg/mL and the solution was irradiated by the 808 nm laser with different power densities of 1, 2, and 3 W/cm^2, respectively. Third, the Au@Res NF solution at a concentration of 200 μg/mL was used to study the photothermal conversion efficiency at a power density of 3 W/cm^2. The laser was applied from 0 s, the laser was removed when the temperature rose to the maximum after 900 s, and the temperature was stopped being recorded at 1800 s.

Toxicity of Au@Res NFs to Normal cells and Cancer Cells. In the cytotoxicity study, L929 cells were selected as the representation of normal cells and A375 cells were selected as the representation of cancer cells. L929 cells and A375 cells were inoculated on 96-well plates at the density of 8000 cells per well. Au@Res NFs with concentrations of 0, 20, 40, 60, 80, 100, 150, and 200 μg/mL were cocultured with these two kinds of cells. After 24 h, the relative cell viability was determined by a CCK-8 assay (WST-8 reduction assay). Each experiment set up five duplicate wells and was repeated three times. It is worth noting that in addition to cells + Au@Res NFs + CCK-8 as the experimental group, we also set (1) cells and (2) Au@Res NFs + CCK-8 as the two control groups. By subtracting the optical density values of the experimental group at 450 nm from the optical density values of the two control groups at 450 nm, the interference of Au@Res NF itself, CCK-8 itself, and the interaction between the two can be eliminated.

Cell Cycle Detected by Flow Cytometry. A375 cells were inoculated on six-well plates at the density of 300,000 cells per well. Au@Res NFs with the concentrations of 0, 25, 50, 75, and 100 μg/mL were cocultured with A375 cells for 24 h. Then, the cells were washed with PBS, fixed with ethanol (70%) for 12 h, washed again with PBS, and incubated with propidium staining solution (containing buffer, propidium, and RNase) at 37 °C in dark. The cell cycle detection was performed by a flow cytometer.

Expression of Apoptosis-Related Proteins. A375 cells were inoculated on 6-well plates at the density of 300,000 cells per well. Au@Res NFs with concentrations of 0, 50, and 100 μg/mL were cocultured with A375 cells for 24 h. Then, the cells were washed with PBS three times and a RIPA-containing protease inhibitor was added. After centrifugation, the supernatant was a protein sample and the concentration of protein was detected by a BCA protein assay kit. The protein samples were denatured, depolymerized by high-temperature treatment (100 °C, 5 min), run on SDS-PAGE, and then transferred to polyvinylidene fluoride membranes. After blocking the membranes with QuickBlock blocking buffer for 1 h, the membranes were washed and incubated with primary antibodies overnight at 4 °C. The following primary antibodies were used: anti-β-tubulin (1:2000), anti-Bax (1:2000), and anti-Bcl2 (1:2000). Subsequently, the membranes were washed and incubated with a secondary antibody (HRP-conjugated Goat Anti-Rabbit IgG(H+L), 1:5000) for 2 h. Finally, the expression of apoptosis-related proteins Bax and Bcl2 was detected by ECL chemiluminiscence.

Cell Apoptosis Detected by Flow Cytometry. A375 cells were inoculated on six-well plates at the density of 300,000 cells per well. Au@Res NFs with the concentration of 50 μg/mL were cocultured with A375 cells, and then the cells were irradiated with an 808 nm laser at different power densities of 0, 0.33, 0.5, 1, and 2 W/cm^2. After 24 h of incubation, the cells were washed with PBS, centrifuged, resuspended with buffer, and stained with Annexin V-FITC and PI. The cell apoptosis was performed by a flow cytometer.

Clonal Formation Experiment. A375 cells were inoculated on six-well plates at the density of 300,000 cells per well. Au@Res NFs with the concentration of 50 μg/mL were cocultured with A375 cells, and then the cells were irradiated with an 808 nm laser at different power densities of 0, 0.33, 0.5, 1, and 2 W/cm^2. After 24 h of incubation, the cell culture medium was discarded and then the cells were washed three times with PBS to remove dead cells, digested, and counted. Finally, 500 living cells were taken out, inoculated on a new six-well plate, shaken gently, and placed in an incubator for further culture. When the number of cells in most of the single clones in the well was more than 50, the culture medium was discarded. The cells were washed with PBS, fixed with 4% paraformaldehyde, washed with PBS, and stained with crystal violet dye. The cells were finally washed with deionized water and photographed with scanner.

Safety Study *In Vivo*. All of the *in vivo* animal experiments related to this work were performed in accordance with the Guidelines for Care and Use of Laboratory Animals of Jilin University and approved by the Animal Ethics Committee of the First Hospital of Jilin University. In the safety study *in vivo*, 10 of the Balb/c mice (18 g, 4 weeks, male) were purchased from Beijing Vital River Laboratory Animal Technology Co., Ltd. Then, five mice were iv injected with 50 μL of saline and another 5 mice were iv injected with 50 μL of Au@Res NF solution (5 mg/mL). Then, 24 h after the injection, the blood of mice was collected for blood glucose, blood fat, liver function, and renal function examinations.

Pharmacokinetic Study *In Vivo*. Tumor models constructed by Balb/c nude mice were used in subsequent experiments in this work. Balb/c nude mice (17 g, 4 weeks old, male) were purchased from Beijing Vital River Laboratory Animal Technology Co., Ltd. After being adaptively fed in an SPF animal laboratory for 1 week, 1,000,000 of A375 cells were subcutaneously injected into the right buttock of the mice to establish tumor models. When the average tumor diameter reached 6 mm, the A375 tumor-bearing mice were iv injected with 50 μL of a Au@Res NF solution (5 mg/mL). Then, 5 μL of blood was collected from the tail at different time points of 0, 0.5, 1, 2, 4, 6, 8, 12, and 24 h. Moreover, all the blood samples were dissolved in aqua regia to test the contents of Au by ICP-AES. After 24 h, the mice were euthanized and dissected, and the heart, liver, spleen, lung, kidney, and tumor were all weighed and then dissolved in aqua regia to test the contents of Au by ICP-AES.

CT Imaging Assay *In Vivo*. In a CT imaging assay *in vivo*, A375 tumor-bearing mice were iv injected with 50 μL of Au@Res NF solution (5 mg/mL). After 24 h, the mice were anesthetized and imaged by a medical CT scanner to study the

https://doi.org/10.1021/acsomega.3c03538
ACS Omega 2023, 8, 34629−34639

accumulation of Au@Res NFs in tumor. The voltage is 60 kV, the electric current is 1 mA, and the radiation dose is 0.1 mGy. There were also A375 tumor-bearing mice injected with saline that were used as control.

Animal Experiments. A375 tumor-bearing mice were randomly divided into five groups when the average tumor diameter reached 6 mm: (1) control group; (2) laser control group; (3) Res group; (4) Au@Res NF group; (5) Au@Res NFs + laser group. In the control group and laser control group, the mice were i.v. injected with 50 μL of saline. In the Res group, the mice were i.v. injected with 50 μL of Res solution (5 mg/mL). In the Au@Res NF group and Au@Res NFs + laser group, the mice were i.v. injected with 50 μL of Au@Res NF solution (5 mg/mL). After 24 h, the tumors of mice in the laser control group and Au@Res NFs + laser group were irradiated by an 808 nm laser at the power density of 0.33 W/cm^2 for 30 min. The long axis length (L: mm) and short axis length (S: mm) of tumors and the weights (g) of the mice were recorded every other day. On the 16th day, all the mice were photographed, euthanized, and dissected. The tumors from each group were photographed and then used for subsequent H&E staining and TUNEL staining, and as for the Au@Res NFs + laser group, one tumor was excised for H&E staining and TUNEL staining 4 h after the irradiation. The major organs were fixed with 10% formalin for subsequent H&E staining to evaluate the long-term safety of the experiment.

Characterization. A JEM-2100F TEM (200 kV) was employed to collect TEM photos. A Malvern Zetasizer Nano ZS was employed to collect hydrate particle size data. A Bruker Vertex 80 V FTIR spectrometer was employed to collect FTIR spectra. A Shimadzu UV-3600 spectrophotometer was employed to collect UV−vis-NIR absorption spectra. Agilent 725 ICP-AES was employed to measure the concentration of Au. An RT-6000 microplate reader was employed to collect optical density values. Beckman Coulter CytoFLEX was employed to flow cytometry analysis. An Olympus FV3000 confocal laser scanning microscope was employed to collect crystal violet-stained images of cells. A Tanon 5200 automatic chemiluminescence image analysis system was employed to collect Western blot band photos. Planmeca cone beam CT (60 kV, 1 mA) was employed to collect CT images. An Olympus IX71 microscope was employed to collect H&E staining and TUNEL staining images.

Statistical Analysis. Analysis of variance (ANOVA) followed by Tukey test for multiple comparisons was performed for the evaluation of statistical significance among different groups. $P < 0.05$ was considered to be statistically significant.

■ ASSOCIATED CONTENT

Supporting Information

The Supporting Information is available free of charge at https://pubs.acs.org/doi/10.1021/acsomega.3c03538.

XRD patterns; photographs of Au@Res NFs in water, saline, PBS, and cell culture medium; hydrated particle size of Au@Res NFs before and after 24 h of incubation in cell culture medium; L929 cells incubated with Au NFs at different concentrations; A375 cells were incubated with resveratrol at different concentrations; the percentage of A375 cells in the S phase of the cell cycle after incubation with Au@Res NFs at different concentrations; the protein expression levels of Bax and Bcl2 in A375 cells after incubation with Au@Res NFs at different concentrations; crystal violet staining used to evaluate the proliferation ability of A375 cells; the blood glucose index of the mice in the control group (injected with saline) and experimental group (injected with Au@Res NFs); the major blood fat indexes of the mice in control group (injected with saline) and experimental group (injected with Au@Res NFs); the major liver function indexes of the mice in the control group (injected with saline) and experimental group (injected with Au@Res NFs); the major renal function indexes of the mice in the control group (injected with saline) and experimental group (injected with Au@Res NFs); images of H&E-stained major organ (heart, liver, spleen, lung, and kidney) slices of the mice in each group after treatment (PDF)

■ AUTHOR INFORMATION

Corresponding Authors

Li Rong − *Department of Plastic Surgery, The First Hospital of Jilin University, Changchun 130021, P. R. China*; Email: rong_li@jlu.edu.cn

Duo Zhang − *Department of Plastic Surgery, The First Hospital of Jilin University, Changchun 130021, P. R. China*; orcid.org/0000-0002-7372-6799; Email: zhangduo@jlu.edu.cn

Authors

Tianye Yang − *Department of Plastic Surgery, The First Hospital of Jilin University, Changchun 130021, P. R. China*; orcid.org/0009-0001-9897-9709

Hui Ren − *Department of Nursing, The First Hospital of Jilin University, Changchun 130021, P. R. China*

Wei Zhang − *Department of Plastic Surgery, The First Hospital of Jilin University, Changchun 130021, P. R. China*

Complete contact information is available at: https://pubs.acs.org/10.1021/acsomega.3c03538

Author Contributions

L.R. and D.Z. supervised and proposed the project. T.Y., L.R., and D.Z. designed and performed the experiments and cowrote the paper. W.Z. participated in the synthesis of nanomaterials. H.R. participated in part of the cell experiments and animal experiments. All authors have given approval to the final version of the manuscript.

Notes

The authors declare no competing financial interest.

■ ACKNOWLEDGMENTS

This work was supported by the Key Research and Development Project in the field of medicine and health of Jilin Provincial Department of Science and Technology (20230204091YY).

■ REFERENCES

(1) Cheng, L.; Wang, C.; Feng, L.; Yang, K.; Liu, Z. Functional Nanomaterials for Phototherapies of Cancer. *Chem. Rev.* **2014**, *114*, 10869−10939.

(2) Wolfbeis, O. S. An Overview of Nanoparticles Commonly Used in Fluorescent Bioimaging. *Chem. Soc. Rev.* **2015**, *44*, 4743−4768.

(3) Wei, X.; Zhang, C.; He, S.; Huang, J.; Huang, J.; Liew, S. S.; Zeng, Z.; Pu, K. A Dual-Locked Activatable Phototheranostic Probe

for BiomarkerRegulated Photodynamic and Photothermal Cancer Therapy. *Angew. Chem., Int. Ed.* **2022**, *61*, 202202966.
(4) Gao, P.; Wang, H.; Cheng, Y. Strategies for efficient photothermal therapy at mild temperatures: Progresses and challenges. *Chin. Chem. Lett.* **2022**, *33*, 575−586.
(5) Dai, H.; Cheng, Z.; Zhang, T.; Wang, W.; Shao, J.; Wang, W.; Zhao, Y.; Dong, X.; Zhong, L. Boron difluoride formazanate dye for high-efficiency NIR-II fluorescence imaging-guided cancer photothermal therapy. *Chin. Chem. Lett.* **2022**, *33*, 2501−2506.
(6) Wang, Y.; Xu, S.; Shi, L.; Teh, C.; Qi, G.; Liu, B. Cancer-Cell-Activated in situ Synthesis of Mitochondria-Targeting AIE Photosensitizer for Precise Photodynamic Therapy. *Angew. Chem., Int. Ed.* **2021**, *60*, 14945−14953.
(7) Yang, Y.; Chen, F.; Xu, N.; Yao, Q.; Wang, R.; Xie, X.; Zhang, F.; He, Y.; Shao, D.; Dong, W.; Fan, J.; Sun, W.; Peng, X. Red-light-triggered self-destructive mesoporous silica nanoparticles for cascade-amplifying chemo-photodynamic therapy favoring antitumor immune responses. *Biomaterials* **2022**, *281*, 121368.
(8) Liang, S.; Xiao, X.; Bai, L.; Liu, B.; Yuan, M.; Ma, P.; Pang, M.; Cheng, Z.; Lin, J. Conferring Ti-Based MOFs with Defects for Enhanced sonodynamic Cancer Therapy. *Adv. Mater.* **2021**, *33*, 2100333.
(9) Tian, H.; Wang, G.; Sang, W.; Xie, L.; Zhang, Z.; Li, W.; Yan, J.; Tian, Y.; Li, J.; Li, B.; Dai, Y. Manganese-phenolic nanoadjuvant combines sonodynamic therapy with cGAS-STING activation for enhanced cancer immunotherapy. *Nano Today* **2022**, *43*, 101405.
(10) Tang, Z.; Liu, Y.; He, M.; Bu, W. chemodynamic Therapy: Tumour Microenvironment-Mediated Fenton and Fenton-like Reactions. *Angew. Chem., Int. Ed.* **2019**, *58*, 946−956.
(11) Dong, S.; Dong, Y.; Liu, B.; Liu, J.; Liu, S.; Zhao, Z.; Li, W.; Tian, B.; Zhao, R.; He, F.; Gai, S.; Xie, Y.; Yang, P.; Zhao, Y. Guiding Transition Metal-Doped Hollow Cerium Tandem Nanozymes with Elaborately Regulated Multi-Enzymatic Activities for Intensive chemodynamic Therapy. *Adv. Mater.* **2022**, *34*, 2107054.
(12) Chang, J.; Qin, X.; Li, S.; He, F.; Gai, S.; Ding, H.; Yang, P. Combining Cobalt Ferrite Nanozymes with a Natural Enzyme to Reshape the Tumor Microenvironment for Boosted Cascade Enzyme-Like Activities. *ACS Appl. Mater. Interfaces* **2022**, *14*, 45217−45228.
(13) Li, S.; Ding, H.; Chang, J.; Dong, S.; Shao, B.; Dong, Y.; Gai, S.; He, F.; Yang, P. Bimetallic oxide nanozyme-mediated depletion of glutathione to boost oxidative stress for combined nanocatalytic therapy. *J. Colloid Interface Sci.* **2022**, *623*, 787−798.
(14) Li, J.; Luo, Y.; Pu, K. Electromagnetic Nanomedicines for Combinational Cancer Immunotherapy. *Angew. Chem., Int. Ed.* **2021**, *60*, 12682−12705.
(15) He, S.; Li, J.; Cheng, P.; Zeng, Z.; Zhang, C.; Duan, H.; Pu, K. Charge-Reversal Polymer Nano-modulators for Photodynamic Immunotherapy of Cancer. *Angew. Chem., Int. Ed.* **2021**, *60*, 19355−19363.
(16) Liu, S.; Zhang, M.; Jin, H.; Wang, Z.; Liu, Y.; Zhang, S.; Zhang, H. Iron-Containing Protein-Mimic Supramolecular Iron Delivery Systems for Ferroptosis Tumor Therapy. *J. Am. Chem. Soc.* **2023**, *145*, 160−170.
(17) Wang, Z.; Wang, L.; Liu, S.; Zhang, M.; Li, Y.; Rong, L.; Liu, Y.; Zhang, H. Z-Scheme heterostructures for glucose oxidasesensitized radiocatalysis and starvation therapy of tumors. *Nanoscale* **2022**, *14*, 2186−2198.
(18) Chen, M.; Tang, S.; Guo, Z.; Wang, X.; Mo, S.; Huang, X.; Liu, G.; Zheng, N. Core-Shell Pd@Au Nanoplates as Theranostic Agents for *In-Vivo* Photoacoustic Imaging, CT Imaging, and Photothermal Therapy. *Adv. Mater.* **2014**, *26*, 8210−8216.
(19) Tong, X.; Wang, Z.; Sun, X.; Song, J.; Jacobson, O.; Niu, G.; Kiesewetter, D. O.; Chen, X. Size Dependent Kinetics of Gold Nanorods in EPR Mediated Tumor Delivery. *Theranostics* **2016**, *6*, 2039−2051.
(20) Song, J.; Yang, X.; Jacobson, O.; Huang, P.; Sun, X.; Lin, L.; Yan, X.; Niu, G.; Ma, Q.; Chen, X. Ultrasmall Gold Nanorod Vesicles with Enhanced Tumor Accumulation and Fast Excretion from the Body for Cancer Therapy. *Adv. Mater.* **2015**, *27*, 4910−4917.
(21) Nakagawa, T.; Gonda, K.; Kamei, T.; Cong, L.; Hamada, Y.; Kitamura, N.; Tada, H.; Ishida, T.; Aimiya, T.; Furusawa, N.; Nakano, Y.; Ohuchi, N. X-ray computed tomography imaging of a tumor with high sensitivity using gold nanoparticles conjugated to a cancer-specific antibody *via* polyethylene glycol chains on their surface. *Sci. Technol. Adv. Mater.* **2016**, *17*, 387−397.
(22) Yang, X.; Yang, M.; Pang, B.; Vara, M.; Xia, Y. Gold Nanomaterials at Work in Biomedicine. *Chem. Rev.* **2015**, *115*, 10410−10488.
(23) Zhao, P.; Liu, S.; Wang, L.; Liu, G.; Cheng, Y.; Lin, M.; Sui, K.; Zhang, H. Alginate mediated functional aggregation of gold nanoclusters for systemic photothermal therapy and efficient renal clearance. *Carbohyd. Polym.* **2020**, *241*, 116344.
(24) Jing, L.; Liang, X.; Deng, Z.; Feng, S.; Li, X.; Huang, M.; Li, C.; Dai, Z. Prussian Blue Coated Gold Nanoparticles for Simultaneous Photoacoustic/CT Bimodal Imaging and Photothermal Ablation of Cancer. *Biomaterials* **2014**, *35*, 5814−5821.
(25) Nikoobakht, B.; El-Sayed, M. A. Preparation and Growth Mechanism of Gold Nanorods (NRs) Using Seed-Mediated Growth Method. *Chem. Mater.* **2003**, *15*, 1957−1962.
(26) Ratto, F.; Centi, S.; Avigo, C.; Borri, C.; Tatini, F.; Cavigli, L.; Kusmic, C.; Lelli, B.; Lai, S.; Colagrande, S.; Faita, F.; Menichetti, L.; Pini, R. A Robust Design for Cellular Vehicles of Gold Nanorods for Multimodal Imaging. *Adv. Funct. Mater.* **2016**, *26*, 7178−7185.
(27) Wang, Y.; Black, K. C. L.; Luehmann, H.; Li, W.; Zhang, Y.; Cai, X.; Wan, D.; Liu, S.-Y.; Li, M.; Kim, P.; Li, Z.-Y.; Wang, L. V.; Liu, Y.; Xia, Y. Comparison Study of Gold Nanohexapods, Nanorods, and Nanocages for Photothermal Cancer Treatment. *ACS Nano* **2013**, *7*, 2068−2077.
(28) Chen, J.; Glaus, C.; Laforest, R.; Zhang, Q.; Yang, M.; Gidding, M.; Welch, M. J.; Xia, Y. Gold Nanocages as Photothermal Transducers for Cancer Treatment. *Small* **2010**, *6*, 811−817.
(29) Lu, S.; Li, X.; Zhang, J.; Peng, C.; Shen, M.; Shi, X. Dendrimer-Stabilized Gold Nanoflowers Embedded with Ultrasmall Iron Oxide Nanoparticles for Multimode Imaging-Guided Combination Therapy of Tumors. *Adv. Sci.* **2018**, *5*, 1801612.
(30) Wu, F.; Liu, Y.; Wu, Y.; Song, D.; Qian, J.; Zhu, B. Chlorin e6 and polydopamine modified gold nanoflowers for combined photothermal and photodynamic therapy. *J. Mater. Chem. B* **2020**, *8*, 2128−2138.
(31) Nel, A.; Xia, T.; Mädler, L.; Li, N. Toxic Potential of Materials at the Nanolevel. *Science* **2006**, *311*, 622−627.
(32) Sharifi, S.; Behzadi, S.; Laurent, S.; Forrest, M. L.; Stroeve, P.; Mahmoudi, M. Toxicity of Nanomaterials. *Chem. Soc. Rev.* **2012**, *41*, 2323−2343.
(33) Liu, S. W.; Wang, L.; Lin, M.; Liu, Y.; Zhang, L. N.; Zhang, H. Tumor photothermal therapy employing photothermal inorganic nanoparticles/polymers nanocomposites. *Chin. J. Polym. Sci.* **2019**, *37*, 115−128.
(34) Yan, J.; Wang, G.; Xie, L.; Tian, H.; Li, J.; Li, B.; Sang, W.; Li, W.; Zhang, Z.; Dai, Y. Engineering Radiosensitizer-Based Metal-Phenolic Networks Potentiate STING Pathway Activation for Advanced Radiotherapy. *Adv. Mater.* **2022**, *34*, 2105783.
(35) Guo, Y.; Jia, H.-R.; Zhang, X.; Zhang, X.; Sun, Q.; Wang, S.-Z.; Zhao, J.; Wu, F.-G. A Glucose/Oxygen-Exhausting Nanoreactor for Starvation- and Hypoxia-Activated Sustainable and Cascade Chemo-chemodynamic Therapy. *Small* **2020**, *16*, 2000897.
(36) Zhang, L.; Wan, S.-S.; Li, C.-X.; Xu, L.; Cheng, H.; Zhang, X.-Z. An Adenosine Triphosphate-Responsive Autocatalytic Fenton Nanoparticle for Tumor Ablation with Self-Supplied H_2O_2 and Acceleration of Fe(III)/Fe(II) Conversion. *Nano Lett.* **2018**, *18*, 7609−7618.
(37) Liu, X.; Liu, J.; Xu, S.; Li, X.; Wang, Z.; Gao, X.; Tang, B.; Xu, K. Gold Nanoparticles Functionalized with Au-Se-Bonded Peptides Used as Gatekeepers for the Off-Target Release of Resveratrol in the Treatment of Triple-Negative Breast Cancer. *ACS Appl. Mater. Interfaces* **2023**, *15*, 2529−2537.
(38) Wang, W.; Tang, Q.; Yu, T.; Li, X.; Gao, Y.; Li, J.; Liu, Y.; Rong, L.; Wang, Z.; Sun, H.; Zhang, H.; Yang, B. Surfactant-Free

https://doi.org/10.1021/acsomega.3c03538
ACS Omega 2023, 8, 34629−34639

Preparation of Au@Resveratrol Hollow Nanoparticles with Photothermal Performance and Antioxidant Activity. *ACS Appl. Mater. Interfaces* **2017**, *9*, 3376−3387.

(39) Li, J.; Han, J.; Xu, T.; Guo, C.; Bu, X.; Zhang, H.; Wang, L.; Sun, H.; Yang, B. Coating Urchinlike Gold Nanoparticles with Polypyrrole Thin Shells To Produce Photothermal Agents with High Stability and Photothermal Transduction Efficiency. *Langmuir* **2013**, *29*, 7102−7110.

https://doi.org/10.1021/acsomega.3c03538
ACS Omega 2023, 8, 34629−34639